crystals

MDPI

*Article*

# High-Field Measurements of CoP and Elemental Combinatorics in the MnP-Type Family

**Daniel J. Campbell [1], John Collini [1,2], Kefeng Wang [1], Limin Wang [1], Brandon Wilfong [1,3], David Graf [4], Efrain E. Rodriguez [1,3] and Johnpierre Paglione [1,5,*]**

[1] Maryland Quantum Materials Center and Department of Physics, University of Maryland, College Park, MD 20742, USA; djcampbe@umd.edu (D.J.C.); jcollini@terpmail.umd.edu (J.C.); kw624@physics.rutgers.edu (K.W.); wanglm@umd.edu (L.W.); bwilfong@umd.edu (B.W.); efrain@umd.edu (E.E.R.)
[2] NIST Center for Neutron Research, National Institute for Standards and Technology, Gaithersburg, MD 20899, USA
[3] Department of Chemistry, University of Maryland, College Park, MD 20742, USA
[4] National High Magnetic Field Laboratory, 1800 East Paul Dirac Drive, Tallahassee, FL 32310, USA; graf@magnet.fsu.edu
[5] Canadian Institute for Advanced Research, Toronto, ON M5G 1Z8, Canada
* Correspondence: paglione@umd.edu

**Abstract**

The MnP family of binary compounds presents an intriguingly simple platform to mix-and-match elemental components. Replacement on the transition metal or pnictogen site can alter magnetism, electronic correlations, and electrical properties. Here we report low-temperature properties of CoP, including measurements at magnetic fields exceeding 30 T, revealing de Haas–van Alphen oscillations and a nearly two orders of magnitude increase in resistance. When viewed together with prior work, it is possible to put together a global picture of the role of different atoms in variations in magnetic ordering, lattice coherence, and topological band structure features in this material family.

**Keywords:** crystal growth; antiferromagnetism; chemical vapor transport; topology

## 1. Introduction

Transition-metal–pnictogen compounds have been well-represented in recent investigations of unconventional superconductivity and topology. Fe-based superconductors are the obvious example [1,2], but 1:1 binaries are intriguing on their own. All of the 3*d* transition metals from Cr to Co form in the same orthorhombic *Pnma* lattice with either P or As (though MnAs only has the *Pnma* lattice from 40 to 125 °C) [3,4]. This is known as the MnP-type structure. VAs is also allowed in this structure, as are heavier metals—RuP, the four (Ru/Rh)(As/Sb) combinations [5] and WP [6]. The various combinations settle into a range of ground states. Mn, Cr, and Fe compounds all have a stable, low-temperature magnetic order [7]. Superconductivity is found in WP [6] through doping in the $Ru_{1-x}Rh_x(P/As)$ series [5] or by applying pressure to CrAs and MnP [8–11], with an overall maximum $T_c$ of 3.7 in $Ru_{0.55}Rh_{0.45}P$. The latter two examples exhibit phase diagrams reminiscent of those seen in unconventional Fe–pnictide, cuprate, and heavy fermion superconductors. Theoretical work has shown that topological features in the band structure should be preserved by this structure [12], and linear magnetoresistance with possible links to linear dispersions has been observed in CrAs [13] and FeP [14].



Academic Editor: Arcady Zhukov

Received: 1 April 2026
Revised: 27 April 2026
Accepted: 28 April 2026
Published: 1 May 2026

Clearly, the choice of elements within the MnP family is central to the properties of the resulting compound. This is not as trivial a finding as it may seem. The pnictogen atoms are ostensibly the same in terms of charge transfer. Going across the 3*d* metals, ground states change from low-temperature spin density waves in Fe compounds [7,15] to paramagnetic Co equivalents [16] and paramagnetic NiAs, which takes on an eponymous hexagonal structure [3]. An overall survey of the trends in this family is important to examining what stabilizes different magnetic and structural ground states.

While much effort has been dedicated to examining the properties of most of the other MnP-type materials [6,10,13,14,16–21], CoP has not received as much attention, with the only reports focusing on crystal growth [22] and magnetic or structural properties mostly at or above room temperature [3,23]. Here we present data from 300 K down to liquid helium temperatures, including the electrical resistance and magnetic torque in magnetic fields above 30 T. High-field measurements have previously been helpful in understanding electronic structures in this family [14,16,18,19,24,25]. We report the dependence of quantum oscillations in magnetic torque on angle, temperature, and magnetic field. We show that CoP, like its sibling compounds, has extremely large magnetoresistance, increasing to more than 80 times $\rho$(0 T) by 31 T. Combining these new results with previous work on this family, we can take a broader look at the various permutations of transition-metal and pnictogen atoms. This helps pin down the origins of certain properties and find general trends in this system. We find, for example, that high magnetoresistance is independent of low-temperature magnetic states, and that phosphides generally seem to result in better-quality crystals than arsenides. These may be useful for narrowing down possibilities for future research directions.

## 2. Crystal Growth

Like most other materials in the MnP family [6,16,26,27], CoP can be grown by chemical vapor transport (CVT) with $I_2$ as the transport agent [28]. In our case, a quartz tube half the length of a single zone tube furnace was sealed under vacuum with about 1 mg/cm$^3$ of iodine, and the reactants were placed at the hot end of the furnace; the $I_2$ serves to transfer material in the gas phase and deposit it as a single crystal at the cold end. Prior work on the growth of CoP reported a comparison of $I_2$-transported CVT growth using a stoichiometric elemental ratio to that using prereacted powder [22], revealing larger transfers using the former setup. However, in this study, we looked for crystal quality rather than size and found similar quality from both methods, as judged by the residual resistivity ratio (RRR, calculated as $\rho(300\ \mathrm{K})/\rho_0$). Hot end temperatures ranging from 900 °C to 1025 °C (with the end of the furnace generally about 200 °C colder) had no obvious impact on the results of growths, which were left long enough at $T_{max}$ (typically 10–14 days) for all material to react. Lattice parameters from powder XRD of ground crystals are $a$ = 5.08 Å, $b$ = 3.28 Å, and $c$ = 5.59 Å, in agreement with a previous report [3].

## 3. Physical Properties

The resistivity of CoP has a similar temperature dependence to that of CoAs [16], with an initial linear decrease from room temperature indicative of dominant electron–phonon scattering, followed by flattening out at lower temperatures (Figure 1a) when temperature-independent impurity concentration is the primary source of scattering. The residual resistivity at 1.8 K is about 0.5 μΩ cm for the best samples, a factor of 2–4 lower than was seen in CoAs, similar to the improved RRR and $\rho_0$ values of both CrP and FeP in comparison to CrAs and FeAs [13,18,19]. This general trend is consistent with overall observations of lower impurity scattering in phosphide binaries as compared to arsenides.

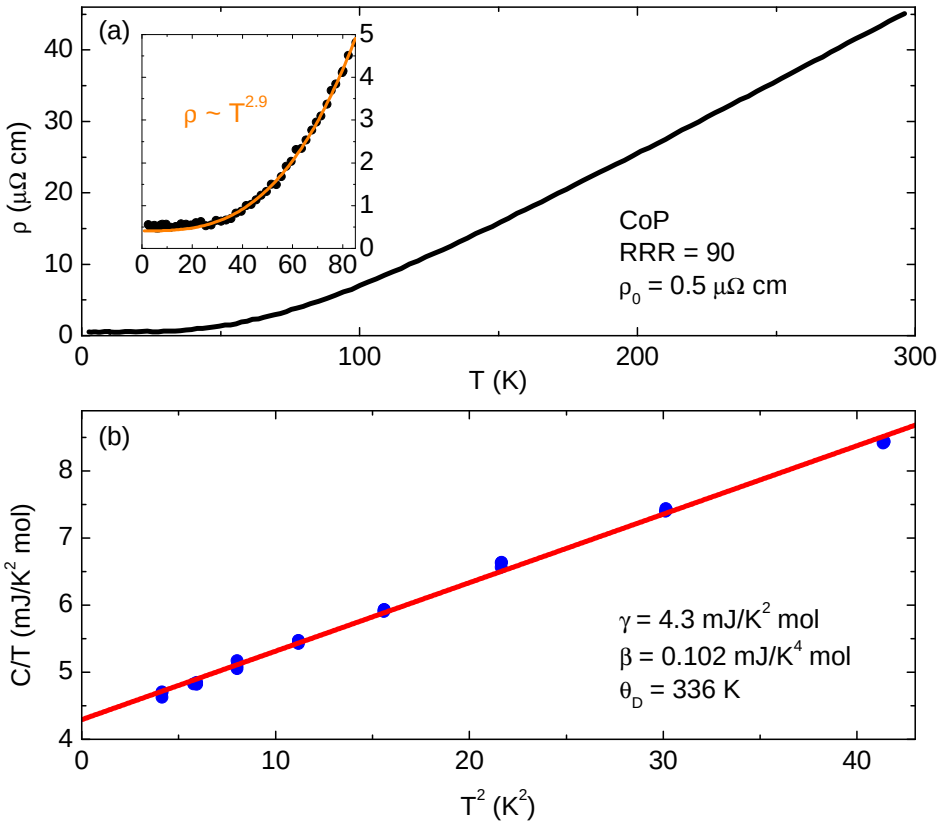


**Figure 1.** (**a**) Electrical resistivity as a function of temperature for a CoAs single crystal. The inset shows a power law fit (orange line) of data in the range 20–80 K, yielding exponent $n = 2.9$. (**b**) Low-temperature specific heat of a CoP single crystal. The red line is a fit to the low-temperature Debye model, and the extracted parameters from the fit are given.

Specific heat measurements were performed down to 1.8 K. The data, when plotted as $C/T$ vs. $T^2$, can be fit to a straight line, in accordance with the low-temperature Debye model $C/T = \gamma + \beta T^2$. Here the Sommerfeld coefficient $\gamma = 4.3\ \frac{\text{mJ}}{\text{K}^2\ \text{mol}}$, slope $\beta = 0.102\ \text{mJ/K}^4\ \text{mol}$ and Debye temperature $\theta_D = (\frac{12\pi N k_B}{5\beta})^{1/3} = 336$ K (Figure 1b), with $N = 2$ the number of atoms per unit cell and $k_B$ the Boltzmann constant. These extracted values are partially lower than the values measured in both CoAs and FeAs [16,29].

Transport measurements up to 31 T were made at the DC Field Facility of the National High Magnetic Field Laboratory (NHMFL). Magnetoresistance (MR, defined as $\frac{\rho(B)-\rho(0\text{T})}{\rho(0\ \text{T})}$) is very large in CoP, reaching 100 times the zero-field resistivity value by 31 T at low temperature (Figure 2). This is another trait that seems to be a general trend with the phosphides of this group, as all of FeP, MnP, and CrP have much larger MR than their arsenide counterparts [13,18,19,25]. This can be at least partially attributed to the lower residual resistivity of the phosphides, which will generally lead to larger MR [30]. It is also a sign that large MR in the other compounds is not a result of magnetism, as while FeP and MnP have complex magnetic orderings, CrP and CoP are both paramagnetic [see SI for the magnetic susceptibility of CoP]. MR is large and nonsaturating in these compounds at all angles, regardless of anisotropies that could be introduced by a magnetic ordering wavevector. Similar to the case for FeP, the lowest MR increase in CoP is observed for fields directed near the *c*-axis. The inset of Figure 2 presents MR angular dependence taken at 31 T, highlighting a sharp reduction in MR within a narrow angular window near the *c*-axis. The minimum value at 31 T occurs at approximately $-5^\circ$ from the *c*-axis, though this may arise from slight misalignment of either the rotator or the sample. While measurements were not taken with similarly fine angular resolution near $B \parallel a$, the observed decrease in

MR at 86° suggests that a comparable effect may occur in that orientation. This behavior contrasts with FeP, where a field directed along $B \parallel a$ produces the maximum MR. In all cases, the curves display a gradual crossover to linear behavior at high fields, consistent with observations in FeAs and FeP.

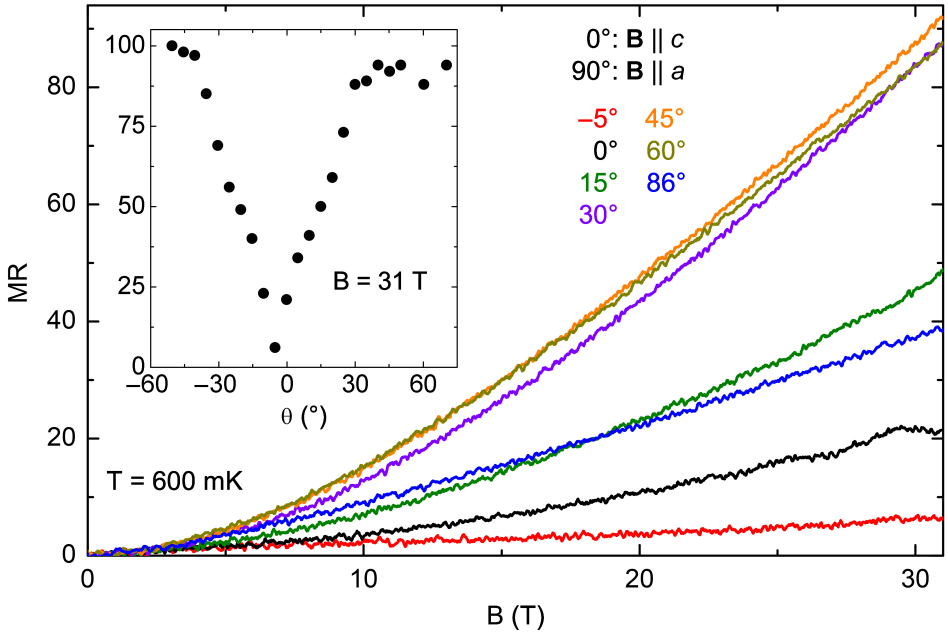


**Figure 2.** High-field magnetoresistance of CoP measured with magnetic field transverse to current orientation, at constant temperature of 600 mK. Angle of field orientation is rotated from *c*-axis (0°) to *a*-axis (90°). The inset presents magnetoresistance as a function of angle at a constant field of 31 T, taken from field sweep data. Note that the 0° curve may exhibit Shubnikov–de Haas oscillations.

## 4. Quantum Oscillations

Quantum oscillations (QOs) were seen in the magnetic torque $\tau = M \times H$, measured via piezoresistive cantilevers [31,32]. These cantilevers are very sensitive and, in the MnP family, have been able to detect QOs in situations where they are not visible in electrical transport [16,18].

We attached a CoP crystal to a cantilever on a uniaxial rotator on two different occasions at the NHMFL, with the field rotating in the orthogonal *ab* and *bc* planes. Oscillatory behavior is clear as low as 5 T (Figure 3a,b). Subtraction of a polynomial fit to the data leaves a purely oscillatory signal, which can be interpolated in $1/B$ and converted to a frequency spectrum with a fast Fourier transform (Figure 3c,d).

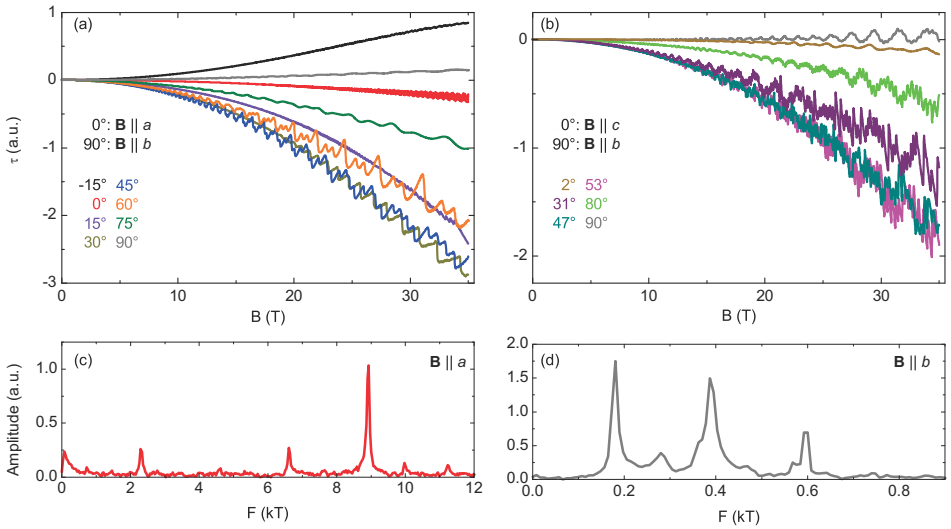


**Figure 3.** Torque magnetometry study of CoP measured up to 35 T, with field orientation rotated to sweep through both the *ab* (panel (**a**)) and *bc* (panel (**b**)) planes, using the same crystal sample for both measurements and presenting a representative set of a more complete angular data set. Lower panels present the frequency analysis using Fourier tranforms of the residual oscillatory signal obtained via polynomial subtraction. Panels present 0° (**c**) and 90° (**d**) obtained from data in (**a**). In (**d**), the frequency range has been truncated for ease of reading, eliminating some lower amplitude peaks at high frequency.

### *4.1. Angular Dependence*

For both rotation planes, there are clear changes in the oscillation pattern with orientation. The resultant map of the observed frequencies is plotted versus the angle in Figure 4 for both angle sweep directions. Both panels have Greek letters marking filled symbols corresponding to what we suspect to be the individual cyclotron orbits. Number subscripts separate peaks that are very close together with similar angular dependence, and thus may stem from the splitting of a single peak. Other peaks have frequencies corresponding to integer multiples or combinations of the labeled peaks, and are therefore likely harmonics or combinations of different 2D orbits around Fermi surface pockets; these are marked with hollow symbols. Without theoretical input, there is no way to confirm our assignment of oscillation frequencies, and there is also no way to relate peaks that appear in the separate oscillation planes except for $\alpha$ $\beta$, and their harmonics, which were observed at the mutual **B** $\parallel$ $b$-axis angle. Note that two $\zeta$ peaks and $\mu$ only appeared in one measurement. The torque is minimal when the field is along crystal axes, so it is possible that, in some measurements, lower amplitude peaks (which these were) do not appear.

Most of our presumed independent frequencies ($\alpha$ being an exception) do not change value significantly with angle, in part because they appear only over a limited angular range. It is possible that, due to a lack of theoretical input, peaks we have identified with different letters actually correspond to a single orbit. That being said, FeP also has a large number of frequencies, very few of which are observed at all angles [33]. The limited angular range of QOs indicates lowered dimensionality of Fermi surface pockets, expected to be a generic feature of MnP-type materials [12]. The presence of such pockets leads to open carrier orbits when the field is perpendicular to a direction in which the pocket extends infinitely, so QOs will not occur. Such open orbits also lead to nonsaturating, and frequently large, magnetoresistance [30].

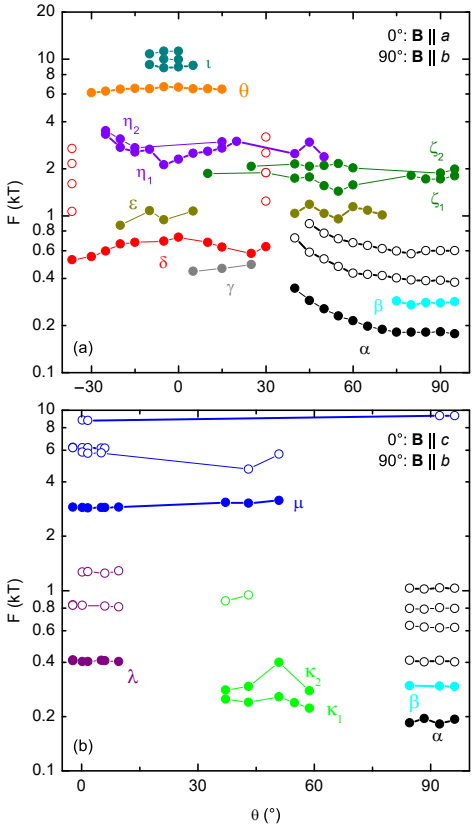


**Figure 4.** Angle dependence of quantum oscillation frequencies in CoP field orientations rotated in the *ab* (panel (**a**)) and *bc* (panel (**b**)) planes. Suspected independent cyclotron orbits are marked with filled symbols, Greek letters, and differing colors; suspected harmonics are unlabeled with hollow symbols.

A large number of quantum oscillation frequency harmonics can arise when carriers make multiple circuits around Fermi surface pockets without being scattered; in the case of CoP, with observations of up to four harmonics in some cases, this scenario would be consistent with the observed low values of residual resistivity. The largest apparently independent frequency we observe, $\delta$, occupies about 30% of the $k_b - k_c$ plane for field along the *c*-axis. This is comparable, for example, to the pocket size seen in FeAs for some field configurations [18].

### *4.2. Temperature and Field Dependence*

With increasing temperature, Landau levels broaden and oscillation amplitude decreases as $R_T = \frac{\alpha m^* T/(Bm_e)}{\sinh(\alpha m^* T/(Bm_e))}$, with $\alpha = 2\pi^2 c k_B/e\hbar \approx 14.69$ T/K, with speed of light *c*. By fitting the change in amplitude with temperature, it is possible to extract the effective mass for a specific oscillation frequency, $m^*/m_e$. Due to the presence of several frequencies in each measurement, we compare FFT amplitudes after an identical extraction procedure. A comparison of the temperature dependence was performed for the *a*-*b* rotation measurements with **B** along [100], [110], and [010], with results shown for **B** $\parallel$ *b*-axis in Figure 5 and Table 1. We tracked only the largest amplitude peak for **B** $\parallel$ [100] and [110] due to the low amplitudes of other peaks. For **B** $\parallel$ [010], the low-frequency oscillation effective masses increase with frequency, as expected for harmonics of a single fundamental. The two high-frequency peaks have similar $m^*$ values, indicating that they might correspond to the splitting of a fundamental frequency. All effective mass values near the electron free mass, though this could be biased by the temperature range we measured over, as orbits with much heavier masses would have immeasurably small amplitude above a few Kelvin.

The effective masses obtained via QOs offer another way to calculate the Sommerfeld coefficient $\gamma = \frac{\pi N_a k_B^2}{3\hbar^2} a_i a_j \sum m^*$. $a_i$ and $a_j$ are the lattice parameters in the plane perpendicular to field [34]. The values obtained are 2.2, 1.4, and 5.3 mJ/K$^2$ mol for [100]-, [110]-, and [010]-oriented fields. The smaller values obtained for the first two cases, compared to the 4.3 mJ/K$^2$ mol from specific heat, are expected. As noted, several frequencies could not be included due to insufficient data points. In addition, this approach does not account for multiple pockets located at symmetrically equivalent positions in the Brillouin zone. For fields applied along the *b*-axis, only the 180 and 9950 T frequencies were used, as the remaining four observed peaks are likely harmonics or split features rather than evidence of additional carriers. The resulting value is slightly higher than that from specific heat measurements, suggesting that no significant orbits are missing and supporting the interpretation that the other FFT peaks arise from harmonics.

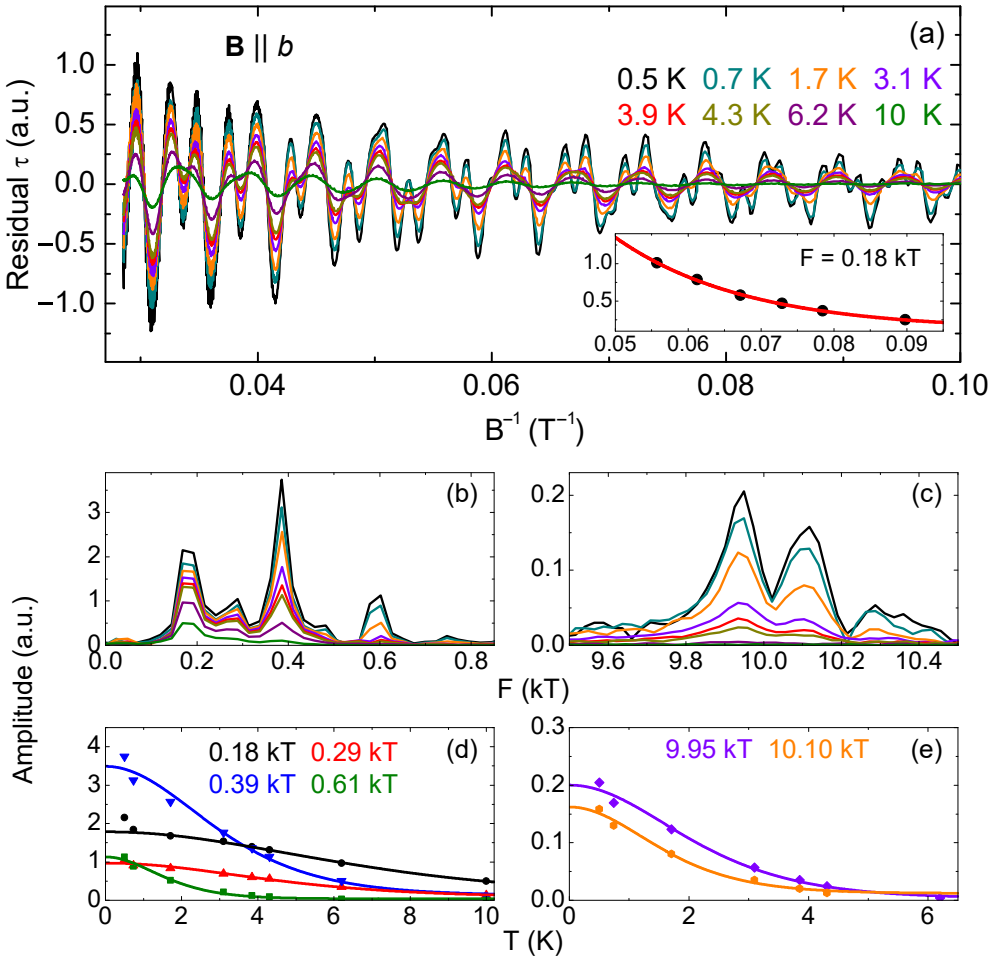


**Figure 5.** Analysis of oscillatory component of torque signal in CoP. Panel (**a**) presents subtracted amplitude at various temperatures for **B** ∥ *b*-axis, with inset showing Dingle factor fit of the lowest frequency (180 T) oscillation. Panels (**b**,**c**) present the Fourier analysis of oscillations at low (**b**) and high (**c**) frequencies for temperatures presented in panel (**a**). Lifshitz–Kosevich analysis of the amplitude temperature dependence is presented for low (**d**) and high (**e**) frequency oscillation bands as labeled, with solid lines indicating fits as described in the text.

**Table 1.** Quantum oscillations fit parameters from CoP torque oscillation data for different magnetic field orientations, including results from fits shown in Figure 5d,e. Some of these frequencies are integer multiples of a lower frequency, and have been labeled as such. As noted, 605 T could be either the second harmonic of $\beta$ or the third harmonic of $\alpha$.

| B ‖ [hkl] | ID | F (T) | $m^*/m_e$ | $T_D$ (K) |
|---|---|---|---|---|
| [100] | $\iota$ | 8,910 | 1.21 | 6.99 |
| [110] | $\alpha$ | 295 | 0.46 | 4.99 |
| [010] | $\alpha$ | 180 | 0.49 | 7.71 |
| [010] | $\beta$ | 290 | 0.61 | — |
| [010] | $2\alpha$ | 390 | 0.94 | — |
| [010] | $3\alpha$ or $2\beta$ | 610 | 1.73 | — |
| [010] | $\mu$ | 9,950 | 1.39 | — |
| [010] | $\lambda$ | 10,100 | 1.61 | — |

The field dependence of a cyclotron orbit is encompassed by the Dingle factor, $R_D = \exp[-\alpha m^* T_D/(Bm_e)]$, where $T_D$ is the Dingle temperature, a parameter with units of temperature that quantifies the scattering rate. Since calculation of $T_D$ requires that the corresponding frequency dominate the spectrum, we can only extract three $T_D$ values (Figure 5a). $T_D$ values for CoP are middling compared to those found in each of FeAs and CoAs [16,18]. However, the lighter effective masses in CoP mean that the mean free path $\ell \propto m^* T_D$ will be longer. This fits well with the large number of harmonics in the QO spectrum, the low effective carrier masses, and lower residual resistivity in CoP, all of which support the idea that the P-containing compounds are in some sense "cleaner" than the As-containing ones. This is not merely due to different growth methods, but also due to the fact that phosphides are generally grown via vapor transport and arsenides using flux growth, with the former potentially helping to avoid impurities. The lowest residual resistivity in FeAs comes using a Bi flux method [18] rather than CVT, but remains higher than that of FeP.

## 5. Discussion: Comparing MnP-Type Compounds

The results in this work can be put in the context of the entire MnP family. As noted, Cr, Mn, Fe, and Co monophosphides have considerably reduced scattering, which serves to increase their MR. One potential basis for this difference is the increase in spin–orbit coupling when moving to heavier atoms. It has been shown theoretically that spin–orbit coupling substantially affects band splitting and topology in this class of materials [12,35]. We note that all of the effective masses we observed in CoP were close to or even lower than $m_e$, and in FeP, the fundamental frequencies not corresponding to harmonics or magnetic breakdown were similarly below $2m_e$ [33]. In contrast, CoAs and FeAs had $m^*$ that could be more than double that [16,18], indicative of the difference in correlated electron behavior between phosphides and arsenides. Indeed, one work found it necessary to account for SOC to explain the magnetic ordering found in FeAs [36].

The magnetoresistance across the MnP family provides evidence for open Fermi surfaces. An early magnetoresistance study of MnP speculated that nonsaturating MR was seen because the high field limit ($\omega_c \tau \gg 1$) was not reached. But by this point, many MnP-type compounds have been measured in high (>30 T) magnetic fields without saturation of the MR at any angle [14,16,18,19,37], despite quantitatively reaching that limit. For example, for CoP, an FS pocket leading with a 1 kT oscillation frequency will reach a value of $\omega_c \tau$ above 50 by 10 T. A logical explanation is that there are open orbits on the FS, which will lead to nonsaturating MR. Calculations focusing on CrAs, MnP, and WP predict coexistence of 2D and 3D FS elements [12]. The concomitant observation of nonsaturating MR quantum oscillations, which require closed orbits, in CrAs, CrP, MnP, FeP, FeAs, CoP,

and CoAs [13,14,16,18,19,25], is a sign of the coexistence of two- and three-dimensional pockets. The same theoretical work noted that, due to the nonsymmorphic nature of the MnP structure, certain features in the band dispersion were required by symmetry considerations, regardless of specific chemical composition. A dispersion linear in one direction but quadratic in another is thought to give rise to linear MR for $\mathbf{B} \parallel c$-axis in FeP and (under pressure) CrAs [13,14]. Even other binary pnictides tend to have a $B$-linear dependence at high enough fields [14,18,19,25,37]. We speculate that common band dispersion features, such as the presence of both 2D and 3D pockets and the "semi-Dirac point" most prominently highlighted in CrAs and FeP, lead to common features in the magnetoresistance of many MnP-type materials.

Table 2 lists the lattice parameters of all MnP-type materials and whether or not they possess long-range magnetic order. For the pnictogens, behavior is simple: a larger atom increases lattice size in all three directions. The story is more complex for the transition-metal site. Moving to the right generally increases $a$ and $c$ and decreases $b$, but exceptions can be found. This general pattern increases the distortion to the "ideal" structure [12] where $a = c = b\sqrt{2}$. In line with that, moving from Cr to Co, magnetic correlations weaken, with transition temperatures decreasing (compare $T_N = 270$, 120, and 70 K in CrAs, FeP, and FeAs [7]) before eventually disappearing altogether. This does not explain everything, as the lattice parameters of CrAs and FeP are near the opposite ends of the range of the 3*d*-containing compounds. But we note also that CrAs undergoes an increase in $a$- and $c$-axis length and a sharp $b$-axis contraction under pressure as the magnetic state is suppressed and superconductivity emerges [38], moving it further from the "ideal" structure. WP, the only stoichiometric, ambient-pressure superconductor in this family, also has the largest $c/b$ ratio (while RhAs and RhBi have been reported to be superconductors [39], we find no evidence for this, as seen in the SI). Hydrostatic or uniaxial pressure studies, the latter of which would be especially useful for tuning axis ratios, could give further insight into the trends linking crystal structure, magnetism, and possible unconventional superconductivity in this family.

**Table 2.** Comparison of structural parameters and magnetic ordering for compounds of the MnP family. Details on growth and basic properties of RhAs and RhSb can be found in the Supplemental Information. Materials marked with an asterisk (*) are known (or suspected for the case of RhAs—see SI for details) to exhibit a structural transition to the hexagonal NiAs structure at high temperatures (i.e., >900 °C) [40]. Note that lattice parameters have been rounded to two decimal places for convenience.

| Formula | *a* (Å) | *b* (Å) | *c* (Å) | Mag. Order |
|---|---|---|---|---|
| VAs [21] | 5.85 | 3.37 | 6.29 | No |
| CrP [41] | 5.36 | 3.11 | 6.02 | No |
| *CrAs [42] | 5.65 | 3.46 | 6.21 | $T_N = 264$ K |
| MnP [10] | 5.26 | 3.17 | 5.92 | $T_C = 291$ K, $T_N = 50$ K |
| MnAs [4] [1] | 5.72 | 3.68 | 6.38 | No [2] |
| FeP [14] | 5.10 | 3.10 | 5.79 | $T_N = 120$ K |
| FeAs [18] | 5.44 | 3.37 | 6.02 | $T_N = 70$ K |
| CoP | 5.08 | 3.28 | 5.59 | No |
| *CoAs [16] | 5.28 | 3.49 | 5.87 | No |
| MoAs [43] | 5.97 | 3.36 | 6.41 | No |

**Table 2.** *Cont.*

| Formula | *a* (Å) | *b* (Å) | *c* (Å) | Mag. Order |
|---|---|---|---|---|
| RuP [41] | 5.52 | 3.17 | 6.12 | No |
| RuAs [21] | 5.72 | 3.34 | 6.31 | No |
| RuSb [44] | 5.96 | 3.70 | 6.58 | No |
| *RhAs [SI] | 5.65 | 3.60 | 6.06 | No |
| RhSb [SI] | 5.97 | 3.87 | 6.34 | No |
| WP [6] | 5.72 | 3.24 | 6.21 | No |

[1] Only from 40 to 120 °C; hexagonal NiAs structure at room temperature. [2] FM in the NiAs structure at room temperature and below.

## 6. Methods

Powder X-ray diffraction (XRD) measurements were made using Cu $K_\alpha$ ($\lambda$ = 1.5406 Å) radiation. Temperature-dependent transport measurements were made using commercial cryostat systems with magnetic fields up to 14 T. Magnetic susceptibility was measured in a 7 T Quantum Design Magnetic Properties Measurement System. Electrical transport and magnetic torque were measured up to 31 and 35 T, respectively, using two different resistive magnets at the National High Magnetic Field Laboratory's DC Field Facility.

## 7. Conclusions

We have presented data on the low-temperature, high-field electrical and magnetic properties of CoP, which serves as a jumping-off point for a survey of all the MnP-type compounds. We can make some general statements about MnP-type binaries: arsenides show a higher level of correlated-electron behavior than phosphides, leading to heavier carriers, a higher residual resistivity, and a suppression of magnetoresistance. The choice of pnictogen atom seems to be the biggest factor in these three properties, even though ground-state magnetism is determined primarily by the transition metal. Examination of structural trends shows that ordered magnetism is favored with a less distorted unit cell, and though there are fewer examples, the opposite may be true of unconventional superconductivity. This work could serve as motivation for chemical doping or pressure studies, where further lattice tinkering could uncover even more interesting phenomena in this group.

**Supplementary Materials:** The following supporting information can be downloaded at: https://www.mdpi.com/article/10.3390/cryst16050299/s1, Figure S1: magnetic susceptibility of CoP at 5 T; Figure S2: resistivity and specific heat of RhAs and RhSb; References [3,5,6].

**Author Contributions:** Conceptualization, D.J.C. and J.P.; methodology, D.J.C. and J.P.; formal analysis, D.J.C., J.C., K.W., L.W., B.W.; investigation, D.J.C., J.C., K.W., L.W., B.W., D.G.; resources, D.G., E.E.R., J.P.; data curation, D.J.C., J.C., K.W., L.W., B.W.; writing—original draft preparation, D.J.C. and J.P.; writing—review and editing, D.J.C. and J.P.; visualization, D.J.C.; supervision, E.E.R., J.P.; project administration, E.E.R., J.P.; funding acquisition, E.E.R., J.P.; All authors have read and agreed to the published version of the manuscript.

**Funding:** This work was supported by Air Force Office of Scientific Research (award no. FA9550-22-1-0023), National Science Foundation Division of Materials Research (award no. DMR-2303090), the Gordon and Betty Moore Foundation's EPiQS Initiative (through grant no. GBMF9071), and the Maryland Quantum Materials Center. A portion of this work was performed at the National High Magnetic Field Laboratory, which is supported by the National Science Foundation Cooperative (Agreement nos. DMR-1157490 and 1644779) as well as the state of Florida. D.J.C. acknowledges the support of the Anne G. Wylie Dissertation Fellowship.

**Data Availability Statement:** The original contributions presented in this study are included in the article and supplementary material. Further inquiries can be directed to the corresponding author.

**Conflicts of Interest:** The authors declare no conflicts of interest.

## Abbreviations

The following abbreviations are used in this manuscript:

| | |
|---|---|
| FQM2024 | Fundamentals of Quantum Materials Winter School |
| Fe | Iron |
| Al | Aluminum |
| $\rho$ | Resistivity |
| $H$ | Magnetic field |
| $T$ | Temperature |
| $C$ | Heat capacity |
| $M$ | Magnetization |
| DFT | Density functional theory |

## References

1. Paglione, J.; Greene, R.L. High-temperature superconductivity in iron-based materials. *Nat. Phys.* **2010**, *6*, 645. https://doi.org/10.1038/nphys1759.
2. Si, Q.; Yu, R.; Abrahams, E. High-temperature superconductivity in iron pnictides and chalcogenides. *Nat. Rev. Mater.* **2016**, *1*, 16017.
3. Selte, K.; Kjekshus, A.; Andresen, A.F.; Pilotti, Å.; Svensson, S.; Swahn, C.G. Phase Transitions Between the MnP and NiAs Type Structures. *Acta Chem. Scand.* **1973**, *27*, 3195–3206.
4. Wilson, R.H.; Kasper, J.S. The crystal structure of MnAs above 40 °C. *Acta Crystallogr.* **1964**, *17*, 95–101. https://doi.org/10.1107/S0365110X64000330.
5. Hirai, D.; Takayama, T.; Hashizume, D.; Takagi, H. Metal-insulator transition and superconductivity induced by Rh doping in the binary pnictides Ru*Pn* *Pn* = P, As, Sb). *Phys. Rev. B* **2012**, *85*, 140509. https://doi.org/10.1103/PhysRevB.85.140509.
6. Liu, Z.; Wu, W.; Zhao, Z.; Zhao, H.; Cui, J.; Shan, P.; Zhang, J.; Yang, C.; Sun, P.; Wei, Y.; et al. Superconductivity in WP single crystals. *Phys. Rev. B* **2019**, *99*, 184509. https://doi.org/10.1103/PhysRevB.99.184509.
7. Kallel, A.; Boller, H.; Bertaut, E.F. Helimagnetism in MnP-type compounds: MnP, FeP, CrAs and $CrAs_{1-x}Sb_x$ mixed crystals. *J. Phys. Chem. Solids* **1974**, *35*, 1139–1152.
8. Wu, W.; Cheng, J.; Matsubayashi, K.; Kong, P.; Lin, F.; Jin, C.; Wang, N.; Uwatoko, Y.; Luo, J. Superconductivity in the vicinity of antiferromagnetic order in CrAs. *Nat. Commun.* **2014**, *5*, 5508.
9. Kotegawa, H.; Nakahara, S.; Tou, H.; Sugawara, H. Superconductivity of 2.2 K under pressure in helimagnet CrAs. *J. Phys. Soc. Jpn.* **2014**, *83*, 093702.
10. Cheng, J.G.; Matsubayashi, K.; Wu, W.; Sun, J.; Lin, F.; Luo, J.; Uwatoko, Y. Pressure induced superconductivity on the border of magnetic order in MnP. *Phys. Rev. Lett.* **2015**, *114*, 117001.
11. Cheng, J.; Luo, J. Pressure-induced superconductivity in CrAs and MnP. *J. Phys.-Condens. Mat.* **2017**, *29*, 383003. https://doi.org/10.1088/1361-648X/aa7b01.
12. Cuono, G.; Forte, F.; Cuoco, M.; Islam, R.; Luo, J.; Noce, C.; Autieri, C. Multiple band crossings and Fermi surface topology: Role of double nonsymmorphic symmetries in MnP-type crystal structures. *Phys. Rev. Mater.* **2019**, *3*, 095004. https://doi.org/10.1103/PhysRevMaterials.3.095004.
13. Niu, Q.; Yu, W.; Yip, K.; Lim, Z.; Kotegawa, H.; Matsuoka, E.; Sugawara, H.; Tou, H.; Yanase, Y.; Goh, S.K. Quasilinear quantum magnetoresistance in pressure-induced nonsymmorphic superconductor chromium arsenide. *Nat. Commun.* **2017**, *8*, 15358. https://doi.org/10.1038/ncomms15358.
14. Campbell, D.; Collini, J.; Sławińska, J.; Autieri, C.; Wang, L.; Wang, K.; Wilfong, B.; Eo, Y.; Neves, P.; Graf, D.; et al. Topologically driven linear magnetoresistance in helimagnetic FeP. *npj Quantum Mater.* **2021**, *6*, 38.
15. Rodriguez, E.E.; Stock, C.; Krycka, K.L.; Majkrzak, C.F.; Zajdel, P.; Kirshenbaum, K.; Butch, N.P.; Saha, S.R.; Paglione, J.; Green, M.A. Noncollinear spin-density-wave antiferromagnetism in FeAs. *Phys. Rev. B* **2011**, *83*, 134438.
16. Campbell, D.J.; Wang, L.; Eckberg, C.; Graf, D.; Hodovanets, H.; Paglione, J. CoAs: The line of 3*d* demarcation. *Phys. Rev. B* **2018**, *97*, 174410. https://doi.org/10.1103/PhysRevB.97.174410.
17. Khim, S.; Gillig, M.; Klingeler, R.; Wurmehl, S.; Büchner, B.; Hess, C. Unusual magnetotransport properties in a FeAs single crystal. *Phys. Rev. B* **2016**, *93*, 205129.

18. Campbell, D.J.; Eckberg, C.; Wang, K.; Wang, L.; Hodovanets, H.; Graf, D.; Parker, D.; Paglione, J. Quantum oscillations in the anomalous spin density wave state of FeAs. *Phys. Rev. B* **2017**, *96*, 075120. https://doi.org/10.1103/PhysRevB.96.075120.
19. Niu, Q.; Yu, W.C.; Aulestia, E.I.P.; Hu, Y.J.; Lai, K.T.; Kotegawa, H.; Matsuoka, E.; Sugawara, H.; Tou, H.; Sun, D.; et al. Nonsaturating large magnetoresistance in the high carrier density nonsymmorphic metal CrP. *Phys. Rev. B* **2019**, *99*, 125126. https://doi.org/10.1103/PhysRevB.99.125126.
20. Takase, A.; Kasuya, T. Temperature dependences of electrical resistivity in MnP. *J. Phys. Soc. Jpn.* **1980**, *48*, 430–434. https://doi.org/10.1143/JPSJ.48.430.
21. Saparov, B.; Mitchell, J.E.; Sefat, A.S. Properties of binary transition-metal arsenides (TAs). *Supercond. Sci. Tech.* **2012**, *25*, 084016.
22. Schmidt, A.; Glaum, R. Zum chemischen Transport von Cobaltmonophosphid mit Iod. Experimente und Modellrechnungen. *Z. Anorg. Allg. Chem.* **1995**, *621*, 1693–1702. https://doi.org/10.1002/zaac.19956211014.
23. Selte, K.; Birkeland, L.; Kjekshus, A. On the Structural and Magnetic Properties of $Cr_{1-t}Fe_tP$, $Mn_{1-t}Co_tP$, and $Fe_{1-t}Co_tP$. *Acta Chem. Scand.* **1978**, *32*, 731–735.
24. Takase, A.; Kasuya, T. Low Field Magnetoresistances in MnP; Purity Dependences of the Magnetic Phase Diagram. *J. Phys. Soc. Jpn.* **1980**, *49*, 484–488. https://doi.org/10.1143/JPSJ.49.484.
25. Takase, A.; Kasuya, T. High Field Magnetoresistance in MnP. *J. Phys. Soc. Jpn.* **1980**, *49*, 489–492. https://doi.org/10.1143/JPSJ.49.489.
26. Westerstrandh, B.; Lundgren, L.; Gäfvert, U.; Carlsson, B. Magnetic susceptibility resistivity and thermal expansion measurements on FeP. *Phys. Scr.* **1977**, *15*, 276. https://doi.org/10.1088/0031-8949/15/4/009.
27. Binnewies, M.; Glaum, R.; Schmidt, M.; Schmidt, P. *Chemische Transportreaktionen*; Walter de Gruyter: Berlin, Germany, 2011.
28. Campbell, D.J. Electronic and Magnetic Properties of MnP-Type Binary Compounds. Ph.D. Thesis, University of Maryland, College Park, MD, USA, 2019. https://doi.org/10.13016/kwro-6rau.
29. Gonzalez-Alvarez, D.; Grønvold, F.; Falk, B.; Westrum, E.F.; Blachnik, R.; Kudermann, G. FeAs: Heat capacity, enthalpy increments, other thermodynamic properties from 5 to 1350 K, and magnetic transition. *J. Chem. Thermodyn.* **1989**, *21*, 363–373. https://doi.org/10.1016/0021-9614(89)90137-7.
30. Pippard, A.B. *Magnetoresistance in Metals*; Cambridge University Press: Cambridge, UK, 1989; Volume 2.
31. Rossel, C.; Bauer, P.; Zech, D.; Hofer, J.; Willemin, M.; Keller, H. Active microlevers as miniature torque magnetometers. *J. Appl. Phys.* **1996**, *79*, 8166–8173. https://doi.org/10.1063/1.362550.
32. Brugger, J.; Despont, M.; Rossel, C.; Rothuizen, H.; Vettiger, P.; Willemin, M. Microfabricated ultrasensitive piezoresistive cantilevers for torque magnetometry. *Sens. Actuat. A Phys.* **1999**, *73*, 235–242. https://doi.org/10.1016/S0924-4247(98)00240-4.
33. Nozue, T.; Kobayashi, H.; Kimura, N.; Aoki, H.; Kamimura, T. de Haas-van Alphen effect of FeP in double helical magnetic state. *J. Phys. Soc. Jpn.* **2001**, *70*, 192–198. https://doi.org/10.1143/jpsj.70.192.
34. Mackenzie, A.; Julian, S.; Diver, A.; Lonzarich, G.; Hussey, N.; Maeno, Y.; Nishizaki, S.; Fujita, T. Calculation of thermodynamic and transport properties of Sr2RuO4 at low temperatures using known fermi surface parameters. *Phys. C* **1996**, *263*, 510–515. https://doi.org/10.1016/0921-4534(95)00770-9.
35. Cuono, G.; Autieri, C.; Guarnaccia, G.; Avella, A.; Cuoco, M.; Forte, F.; Noce, C. Spin–orbit coupling effects on the electronic properties of the pressure-induced superconductor CrAs. *Eur. Phys. J. Spec. Top.* **2019**, *228*, 631–641.
36. Frawley, T.; Schoonmaker, R.; Lee, S.H.; Du, C.H.; Steadman, P.; Strempfer, J.; Ziq, K.A.; Clark, S.J.; Lancaster, T.; Hatton, P.D. Elucidation of the helical spin structure of FeAs. *Phys. Rev. B* **2017**, *95*, 064424.
37. Campbell, D.J.; Lin, W.-C.; Collini, J.; Eo, Y.S.; Anand, Y.; Saha, S.; Graf, D.; Zavalij, P.Y.; Paglione, J. Enhancement of Superconductivity in WP via Oxide-Assisted Chemical Vapor Transport. *Materials* **2025**, *18*, 4529. https://doi.org/10.3390/ma18194529.
38. Yu, Z.; Wu, W.; Hu, Q.; Zhao, J.; Li, C.; Yang, K.; Cheng, J.; Luo, J.; Wang, L.; Mao, H.k. Anomalous anisotropic compression behavior of superconducting CrAs under high pressure. *Proc. Natl. Acad. Sci. USA* **2015**, *112*, 14766–14770.
39. Raub, C.; Zachariasen, W.; Geballe, T.; Matthias, B. Superconductivity of some new Pt-metal compounds. *J. Phys. Chem. Solids* **1963**, *24*, 1093–1100. https://doi.org/10.1016/0022-3697(63)90022-2.
40. Tremel, W.; Hoffmann, R.; Silvestre, J. Transitions between NiAs and MnP type phases: An electronically driven distortion of triangular (36) nets. *J. Am. Chem. Soc.* **1986**, *108*, 5174–5187.
41. Rundqvist, S. Phosphides of the B31 (MnP) structure type. *Acta Chem. Scand* **1962**, *16*, 287–292.
42. Selte, K.; Kjekshus, A.; Jamison, W.E.; Andresen, A.F.; Engebretsen, J. Magnetic structure and properties of CrAs. *Acta Chem. Scand.* **1971**, *25*, 1703–1714.
43. Kandler, H.; Reiss, B. Zur Kristallstruktur der intermetallischen Phasen MoAs und $Mo_5As_4$. *Z. Naturforsch.* **1966**, *21*, 549–554.
44. Endresen, K.; Furuseth, S.; Selte, K.; Kjekshus, A.; Rakke, T.; Andresen, A.F. MnP Type Structure of RuSb and RhSb. *Acta Chem. Scand.* **1977**, *31*, 249–252.